Flow Turbulence Combust (2015) 94:155–173
DOI 10.1007/s10494-014-9581-1

Mixing Layer Manipulation Experiment

From Open-Loop Forcing to Closed-Loop Machine Learning Control

Vladimir Parezanović · Jean-Charles Laurentie · Carine Fourment · Joël Delville · Jean-Paul Bonnet · Andreas Spohn · Thomas Duriez · Laurent Cordier · Bernd R. Noack · Markus Abel · Marc Segond · Tamir Shaqarin · Steven L. Brunton

Received: 29 December 2013 / Accepted: 25 July 2014 / Published online: 12 December 2014

Abstract Open- and closed-loop control of a turbulent mixing layer is experimentally performed in a dedicated large scale, low speed wind-tunnel facility. The flow is manipulated by an array of fluidic micro-valve actuators integrated into the trailing edge of a splitter plate. Sensing is performed using a rake of hot-wire probes downstream of the splitter plate in the mixing layer. The control goal is the manipulation of the local fluctuating energy level. The mixing layer's response to the control is tested with open-loop forcing with a wide range of actuation frequencies. Results are discussed for different closed-loop control

Carine Fourment and Joel Delville: Deceased 11 July 2014.

V. Parezanović (✉) · J.-C. Laurentie · C. Fourment · J. Delville · J.-P. Bonnet · A. Spohn · T. Duriez · L. Cordier · B. R. Noack
Institute PPRIME CNRS UPR 3346, 86000 Poitiers, France
e-mail: vladimir.parezanovic@univ-poitiers.fr

M. Abel · M. Segond
Ambrosys GmbH, Potsdam, Germany

M. Abel
LEMTA, Vandoeuvre-lés-Nancy, France

M. Abel
University of Potsdam, Potsdam, Germany

T. Shaqarin
Tafila Technical University, Tafila, Jordan

S. L. Brunton
University of Washington, Seattle, USA

Present Address:
J.-C. Laurentie
Université de Montpellier 2, Montpellier, France

Present Address:
T. Duriez
Laboratorio de FluidoDinamica - Facultad de Ingeneria CONICET - Universidad de Buenos Aires, Ciudad Autonoma de Buenos Aires, Argentina

approaches, such as: adaptive extremum-seeking and in-time POD mode feedback control. In addition, we propose Machine Learning Control (MLC) as a model-free closed-loop control method. MLC arrives reproducibly at the near-optimal in-time control.

Keywords Shear flow · Turbulence · Active flow control · Extremum seeking · POD · Machine learning · Genetic programming

1 Introduction

Controlling the mixing layer properties such as initial transition, turbulence level, expansion rate, redistribution and mixing, is a problem frequently addressed in the literature over several decades. Passive control parameters such as the shape of the trailing edge, the presence of initial span-wise perturbation, the external turbulence level or the presence of longitudinal pressure gradients can have a large influence on the mixing layer's stream-wise evolution [5, 17, 21]. In a zero pressure gradient configuration, numerous experiments have been performed leading to a doubling of the expansion rate of the mixing layer. Open-loop flow control using acoustic perturbations in the plenum chamber, vibrating trailing edge, or synthetic jets at the wall , have been studied. Such control scenarios are based on the excitation of the most amplified initial perturbations which can be directly related to the initial momentum thickness of the boundary layer over the splitter plate [9]. This can lead to actuation on either relatively low frequency [5], or at high frequency [24].

A major issue to be considered in experimental flow control is the definition of the *physical plant* to which the control is applied, *i.e.* what are the boundaries of the physical domain, and what are the possible communications across these boundaries? Some examples of external influences to be taken into account include perturbations of the inflow conditions, sensor drifts and stability of actuator output. A good control process has to be able to deal with such variations, explicitly or even better implicitly. As a consequence, if for a given *plant* an open-loop control is performed and found to be the best, no guaranty exists that this control remains optimal with respect to large or even small external perturbations.

In a mixing layer, the shear created by the difference of external velocities leads asymptotically to a linear stream-wise growth of the mixing layer scales. By nature, this kind of flow is an amplifier of initial perturbations, subject to convective instabilities. The design and optimization of closed-loop control are then challenging. The development of modern actuators, such as micro-valves, piezoelectric, synthetic jets, plasmas, etc. [1, 2, 8], and of real-time systems with a large input/output data rate and computational power, makes it possible to envisage such closed-loop control being performed.

This paper will focus on a simple *plant* featuring an experimental mixing layer flow, where a control is applied at the trailing edge of the splitter plate with the goal of maximizing the turbulent kinetic energy at a given downstream location. The sensors placed at the location of interest, downstream of the trailing edge, are subject to a convective time delay. An essential question is: what useful information is present in the mixing layer flow, and how can it be used in a sensor-based, closed-loop control design? Can we create a framework for a fully automated flow control system, without *a priori* knowledge of the plant properties?

The main features of the experimental installation and the sensor/actuator system are described in Section 2. The wind tunnel conditions are chosen so that the mixing layer flow comprises spatial and temporal scales which can be addressed using the operational performance range of the actuator, and real-time data acquisition/processing systems. An objective function is defined, based on the energy of local velocity fluctuations.

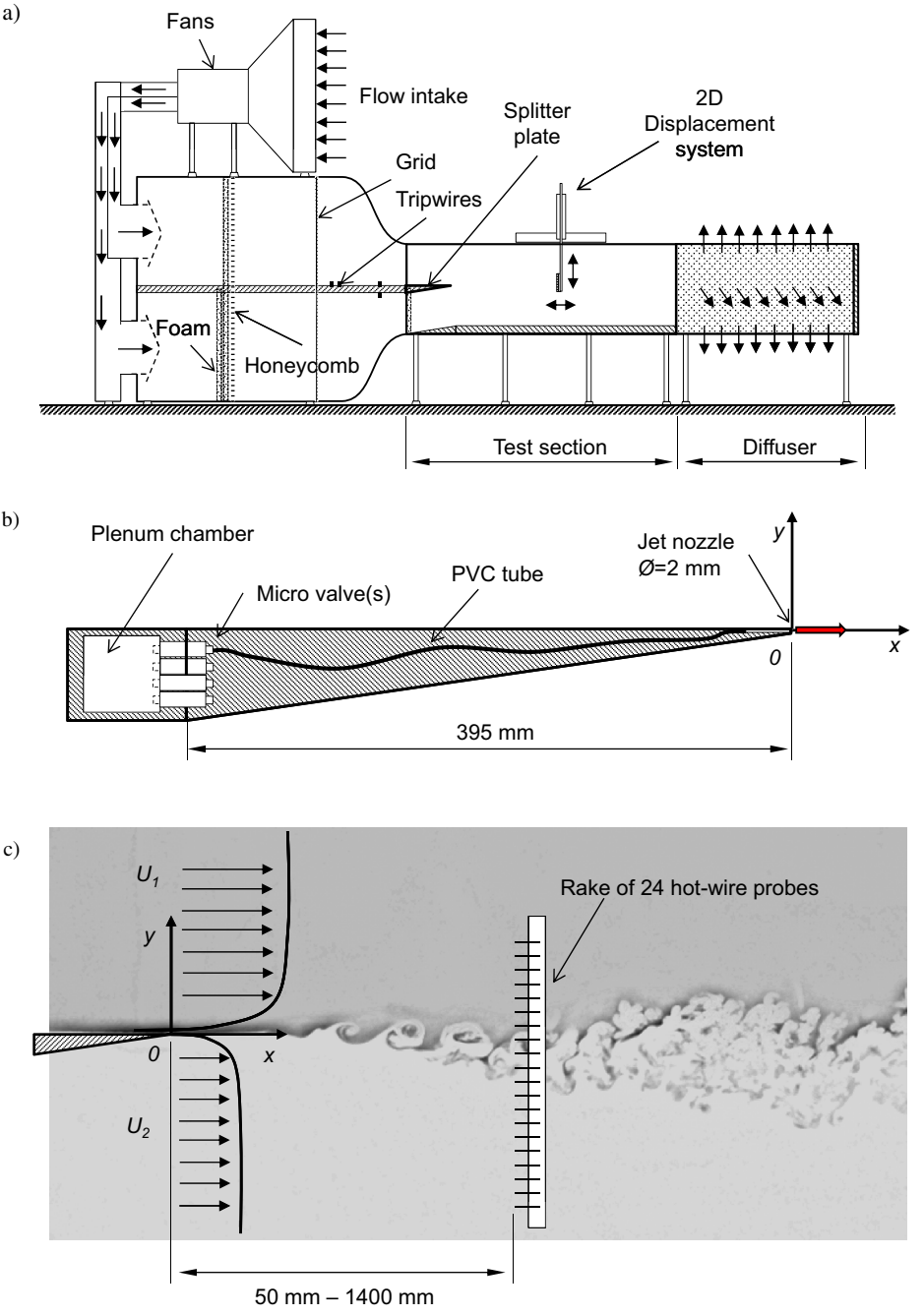

Fig. 1 Experimental setup: **a**) layout of the TUCOROM mixing layer wind tunnel, **b**) a close-up diagram of the splitter plate with the actuation system, and **c**) illustration of the mixing layer flow and sensors

Properties of the un-actuated mixing layer are briefly discussed in Section 3.1. Using a 'blind' open-loop strategy, we show in Section 3.2 that the mixing layer is receptive to the periodic perturbations injected through micro-jets located at the trailing edge of the splitter plate. We compare the resulting effects on the spatial development of the mixing layer with the literature. The impact on the objective function of open-loop actuation frequencies is mapped for one actuation amplitude and duty cycle setting.

In Section 4 we present the methodology and results of several approaches for closed-loop control. Section 4.1 considers an automatic search for the best open-loop actuation frequency by applying an extremum-seeking adaptive control. In Section 4.2, we describe a simple feed-back control, where a POD analysis [16] of the flow at a given stream-wise location is used to provide the control signal for the actuators. The most energetic POD modes can provide information which leads to an enhanced local organization of the mixing layer. Finally, in Section 4.3, a model-free, closed-loop control design is proposed, based on genetic programming [10, 11]. Genetic programming is a function optimization technique belonging to the panoply of biologically-inspired methods from machine learning [23]. We refer to this approach as Machine Learning Control (MLC). This approach is designed to find, in an unsupervised manner, the best sensor-based control law for a given objective function. MLC has been successfully applied to dynamical systems and other experiments [4, 6]. Here, results will be discussed for the transitional mixing layer.

2 Experimental Setup and Measurements

The TUCOROM[1] mixing layer facility, shown in Fig. 1a, is an open-circuit wind tunnel with two driving fans, each generating a separate air stream. The two streams meet at the trailing edge of a splitter plate, and depending on the stream velocity or the type of the splitter plate terminus used, the resulting flow can be either a mixing layer, a step flow or a wake of an infinitely long bluff body. The test section is $l_x \times l_y \times l_z = 3.0\text{m} \times 1.0\text{m} \times 1.0\text{m}$, with a square cross-section. A porous diffuser is used at the outlet of the test section in order to prevent resulting large scale perturbations returning into the inlets. Each stream can be driven independently in a range of velocities $[0.5 : 12]\,\text{ms}^{-1}$. The splitter plate between the two streams is 80mm thick and, in the current configuration, ends with a 3mm thick trailing edge. The taper is introduced only on the lower velocity side of the splitter plate which is angled at 8°, while the upper surface is horizontal. The plane of interest, xy, coincides with the centerline of the splitter plate span, with the origin located at the trailing edge as shown in Fig. 1b. A head loss device (foam) is placed a few centimeters upstream of the bevel in order to stabilize the low velocity stream. This addition limits the maximum operational velocity for the lower stream to $1.7\,\text{ms}^{-1}$.

The trailing edge contains 96 circular nozzles, with a diameter $\phi = 2\text{mm}$, along its span. Each of them is individually connected to a micro-valve actuator, which can be controlled separately. We employ a span-wise mode 0 actuation, where all micro-valves are driven simultaneously by a common square wave signal, of adjustable frequency and duty cycle (dc). The actuators are capable of frequencies higher than 800Hz and of mean exit velocities of the order of the convection velocity of the mixing layer, blowing in the stream-wise direction. The velocity response of the micro-valves, shown in Fig. 2, was characterized with a single miniature hot-wire probe positioned at $x = 1\text{mm}$. At low actuation frequencies the

[1] From ANR project name: "turbulence control using Reduced-Order Models."

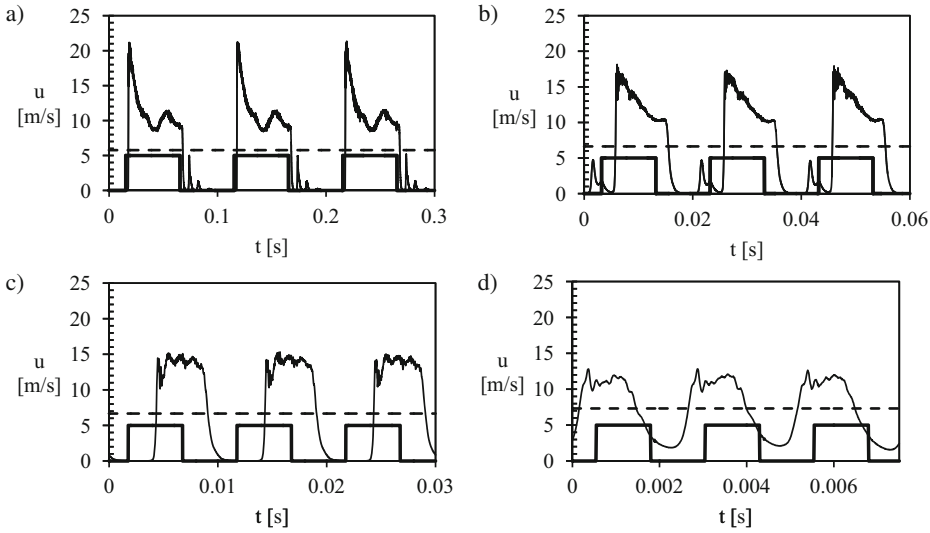

Fig. 2 Velocity response $u_{\text{nozzle}}(t)$ of micro-jet actuators with dc=50 % for actuation frequency f_{a}: **a**) 10Hz, **b**) 50Hz, **c**) 100Hz and **d**) 400Hz. Actuation square wave signal is represented with a thick black line, and the mean nozzle velocity $\overline{u}_{\text{nozzle}}$ with a dashed line

velocity response contains strong transients, while at higher frequencies a response close to a sinusoidal wave is obtained.

Compressed air for the actuators is supplied from a plenum chamber which is also situated in the splitter plate as shown in Fig. 1b. The pressure inside the plenum is controlled, in order to maintain a constant average actuation amplitude. The actuation amplitude in this experiment can be represented by a momentum coefficient $C_\mu = \dot{m}_a/\dot{m}_\theta$, where $\dot{m}_a$ is the mean mass flow rate of air entering the plenum (measured by a flow meter) and $\dot{m}_\theta$ is the mass flow rate through the upper boundary layer. Let θ be the momentum thickness of the boundary layer and l_z the span-wise length of the splitter plate. $\dot{m}_\theta$ is then defined as $\dot{m}_\theta = \rho\theta l_z U_1$. The mass flow rate meter type used is *Brooks* 5863S. The momentum coefficient used is in a range of $0.25 < C_\mu < 0.5$ for different experiments presented.

Measurements comprise Particle Image Velocimetry (PIV) using a *Spectra-Physics Lab-130* Nd:YAG laser, coupled with two *Lavision Image Pro* cameras with an acquisition rate of 5Hz. The PIV cameras are positioned so that the initial part of the developing mixing layer can be observed in a range of $-50\text{mm} < x < 440\text{mm}$. Since smoke visualization uses the same cameras , the covered domains are identical with PIV.

Local velocity measurements are performed using a rake of 24 hot-wire probes (illustrated in Fig. 1c) which can be displaced in a xy plane from $x = 50$ to 1400mm in stream-wise, and $y = \pm 230\text{mm}$ in transverse directions. The two outer hot-wires in the rake are 184mm apart; hence, the rake can cover from 0.5 to 4 times the local thickness of the un-actuated flow, depending on its stream-wise location. The dynamic response of hot-wire anemometers is calibrated up to 20kHz. Each channel is simultaneously sampled at 5kHz. The hot-wire velocity measurements have a precision of 0.05ms^{-1} and are corrected for temperature drifts using a reference temperature sensor at the inlet of the test section. Data acquisition and control are performed by a *Concurrent iHawk* real-time system.

The goal of the control is to maximize the local energy in the mixing layer. The single hot-wire sensors used, provide a measure of the local fluctuating part of the stream-wise component of the velocity. Therefore an objective function J can be introduced as an approximation of the local turbulent kinetic energy:

$$J = \frac{1}{T_\mathrm{J}} \int_0^{T_\mathrm{J}} \left[\sum_{i=1}^{24} u_i'^2(t) \right] \mathrm{d}t, \tag{1}$$

where $u_i'(t)$ is the velocity fluctuation as recorded by the hot-wire anemometer i and $T_\mathrm{J} = 10\mathrm{s}$ is the evaluation time. The mean velocity used for retrieving fluctuations is estimated on $T_\mathrm{mean} = 2\mathrm{s}$ interval. Averaging on a short time scale serves as a high-pass filter to eliminate the contribution of phenomena such as mixing layer flapping in the estimation of energy. This objective function is used to evaluate the efficiency of both open- and closed-loop control approaches presented in this paper. A standard deviation of the objective function for the un-actuated flow J_u is 3 %. This value is calculated on a sample of 50 flow realizations, for a total evaluation time of 500s. Total evaluation time corresponds to 500 cycles of the wind tunnel, based on the convective velocity and the test section length.

3 Mixing Layer Under Periodic Forcing

In Section 3.1 we present the basic features of the un-actuated mixing layer. The response of the mixing layer to periodic forcing is evaluated in Section 3.2 using a few open-loop actuation frequencies from the opposite extremes of the frequency range available to the actuator system. A detailed mapping of the open-loop actuation frequencies is performed and evaluated using the objective function J.

3.1 Un-actuated flow

The initial conditions of the flow used in the experiment are defined as the low speed configuration of $U_1 = 4.7\mathrm{ms}^{-1}$ and $U_2 = 1.2\mathrm{ms}^{-1}$ leading to a velocity ratio $r = 0.255$ and a convective velocity $U_c = (U_1 + U_2)/2 = 2.95\mathrm{ms}^{-1}$. The magnitude of velocity U_1 was selected to provide a stable laminar boundary layer on the upper surface of the splitter plate. The magnitude of U_2 is correspondingly chosen to have a velocity ratio close to r =0.3, taking into account the limitations imposed by the wind tunnel design (see Section 2). The boundary layer on the high speed side of the splitter plate is laminar ($\delta_{99} = 6.9\mathrm{mm}$, $\theta = 0.73\mathrm{mm}$ and $H = 2.44$). The thickness of the boundary layer on the low speed side is $\delta_{99} < 1\mathrm{mm}$, due to very low velocity U_2 and the inserted foam flow stabilizer. The impact of this boundary layer on the development of the mixing layer can be considered negligible. Based on the initial momentum thickness of the upper boundary layer and trailing edge thickness, an initial Reynolds number is estimated as $Re_\theta = U_c\theta/\nu \approx 500$. Various data on the un-actuated case are shown in Figs. 3 to 7 as reference. They will be further commented in the text in comparison to the actuated cases.

3.2 Periodic forcing

Smoke visualization and PIV measurements are performed as a preliminary investigation of the receptivity of the mixing layer to open-loop actuation. Actuation frequencies are selected for this test from two extremes of the actuator system operational range:

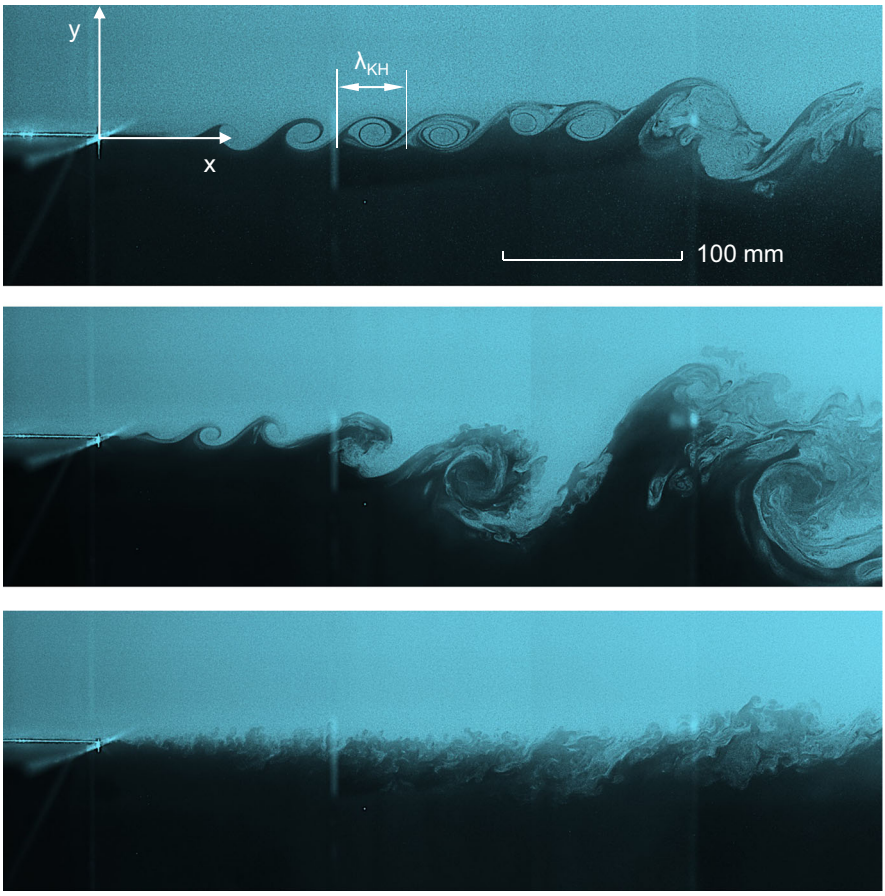

Fig. 3 Smoke/laser visualization of the mixing layer by seeding the top (high speed) stream. The field of view covers −50mm to 440mm in x direction. **a**) un-actuated flow, **b**) low frequency forcing ($f_a = 10$Hz) and **c**) high frequency forcing ($f_a = 400$Hz)

$f_a = 10$Hz and $f_a = 400$Hz. A duty cycle of 50 % is used. Figure 3a shows the un-actuated case, with clearly visible Kelvin-Helmholtz vortices in the initial part of the mixing layer, followed by vortex pairing and a change in the un-actuated mixing layer growth rate. The natural frequency of the mixing layer in the region of the laminar vortices is estimated from the wavelength of the vortices in this picture as $f_{KH} \approx 90$Hz. Actuating at a much lower frequency $f_a \ll f_{KH}$ provokes an earlier creation of larger scale structures (Fig. 3b), while forcing at high frequencies $f_a > f_{KH}$ introduces small scale turbulence immediately downstream of the trailing edge, as shown in Fig. 3c.

The effects on fluctuating quantities in the mixing layer can be observed for all three cases using PIV measurements shown in Fig. 4. The PIV measurements show that actuating at low frequencies increases both stream-wise and cross-stream fluctuations, while the high frequencies have a damping effect.

The hot-wire rake has been used to recover local mean velocity and mean velocity fluctuation profiles in xy plane at various locations downstream of the trailing edge. From

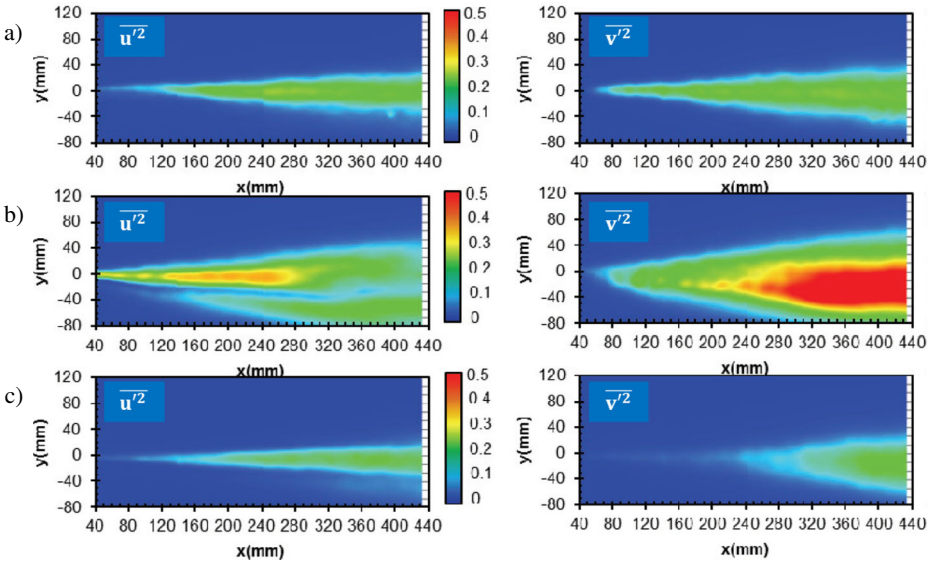

Fig. 4 Mean fields of Reynolds stress components $\overline{u'^2}$ and $\overline{v'^2}$ obtained from PIV on a basis of 300 snapshots: **a**) un-actuated flow, **b**) $f_a = 10$Hz and **c**) $f_a = 400$Hz

the mean stream-wise velocity $U(y)$ profiles we can observe the evolution of vorticity thickness, shown in Fig. 5, and calculated as:

$$\delta_\omega = \frac{U_1 - U_2}{(\partial U/\partial y)_{\max}}. \tag{2}$$

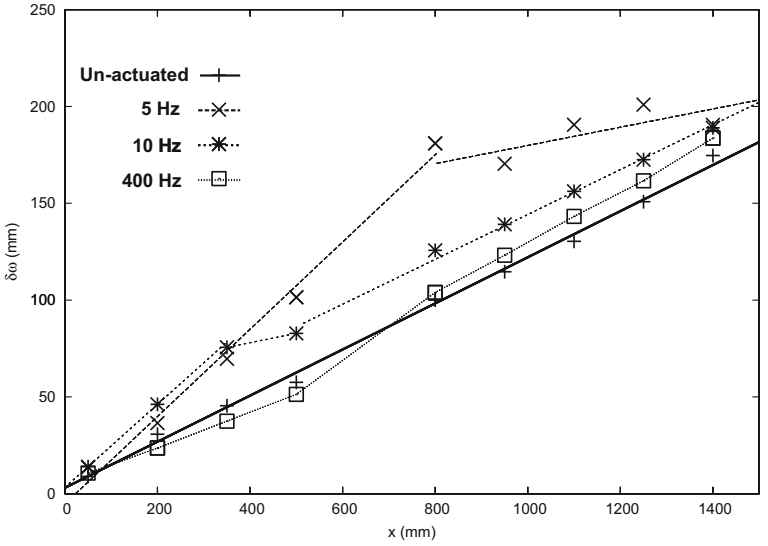

Fig. 5 Influence of the actuation frequency f_a on the local vorticity thickness δ_ω

The un-actuated flow shows a linear evolution of vorticity thickness, with a slope of $\partial\delta_\omega/\partial x = 0.119$ which corresponds well to the data in [5] for similar cases of experimental mixing layers. The low frequency actuation of $f_a = 5$Hz and $f_a = 10$Hz both double the initial vorticity thickness growth rate until $x = 800$mm in the former and $x = 350$mm in the latter case. The high frequency actuation $f_a = 400$Hz initially reduces the vorticity growth rate, but further downstream at around $x = 800$mm, the growth rate changes again ; the vorticity thickness becomes higher compared to the un-actuated flow, but the growth rates are similar in both cases. Such behavior of the forced mixing layer was explored in [20].

These results correspond well with the fact that the actuation affects the transition point of the laminar part of the mixing layer. For the low frequency actuation, the initial part of the mixing layer is dominated by large structures which are created by the tendency of the flow to synchronize itself on the actuation frequencies. For initial stream-wise positions the measurements of the un-actuated flow, shown in Fig. 6, feature energy contained in the broad frequency range up to 100Hz. For $f_a \ll f_{KH}$ the energy in the spectra becomes concentrated at f_a until a certain downstream position, where a re-emergence of base flow frequencies appears. The stream-wise location of these transitions are consistent with the change in vorticity thickness growth rate for corresponding f_a if compared to results in Fig. 5.

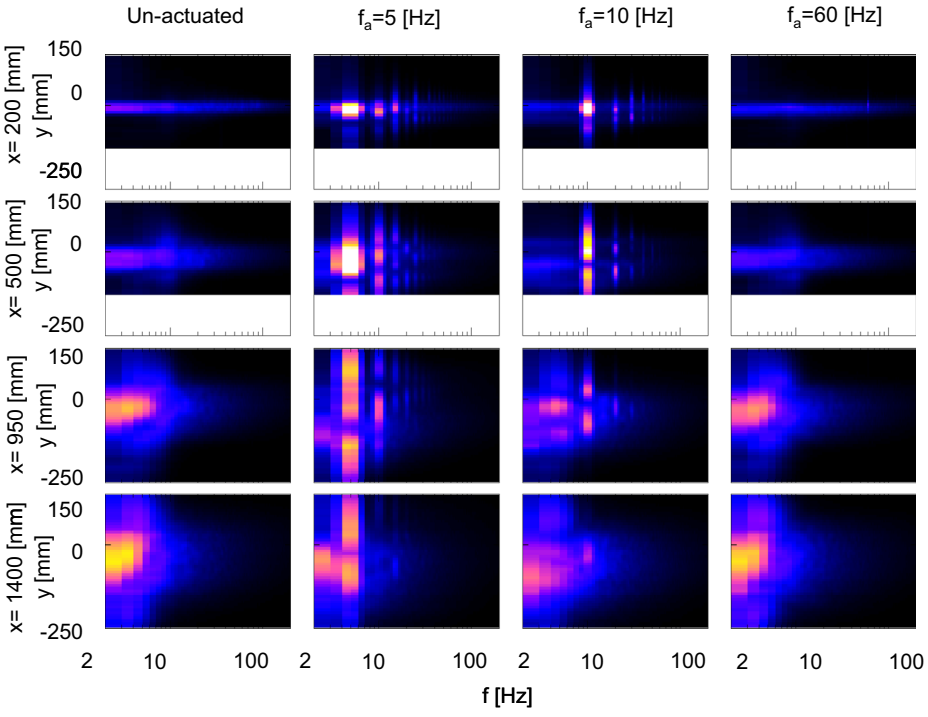

Fig. 6 Spectral maps of the mixing layer for un-actuated flow and open-loop forcing at 5Hz $\leq f_a \leq$ 60 Hz for several stream-wise positions (represented by rows) of the hot-wire rake. Vertical axes denote positions of the hot-wire probes (y_i), horizontal axes frequency range, the color map being the amplitude of the spectra. Case of $f_a = 400$ Hz is omitted here since it is almost identical to the un-actuated spectra

The same behavior is observed from the distribution of fluctuation energy shown as $\overline{u'^2}/\Delta U^2$ in Fig. 7, where $\Delta U^2 = (U_1 - U_2)^2$. An initial linear growth features energy contained in a single, well defined peak (Fig. 7a for x from 200mm to 500mm). In the regions of the first growth rate change, the fluctuation energy profiles feature two or more peaks, as can be seen for $f_a = 5$Hz between $x = 1000$mm and $x = 1400$mm. Around $x = 1400$mm

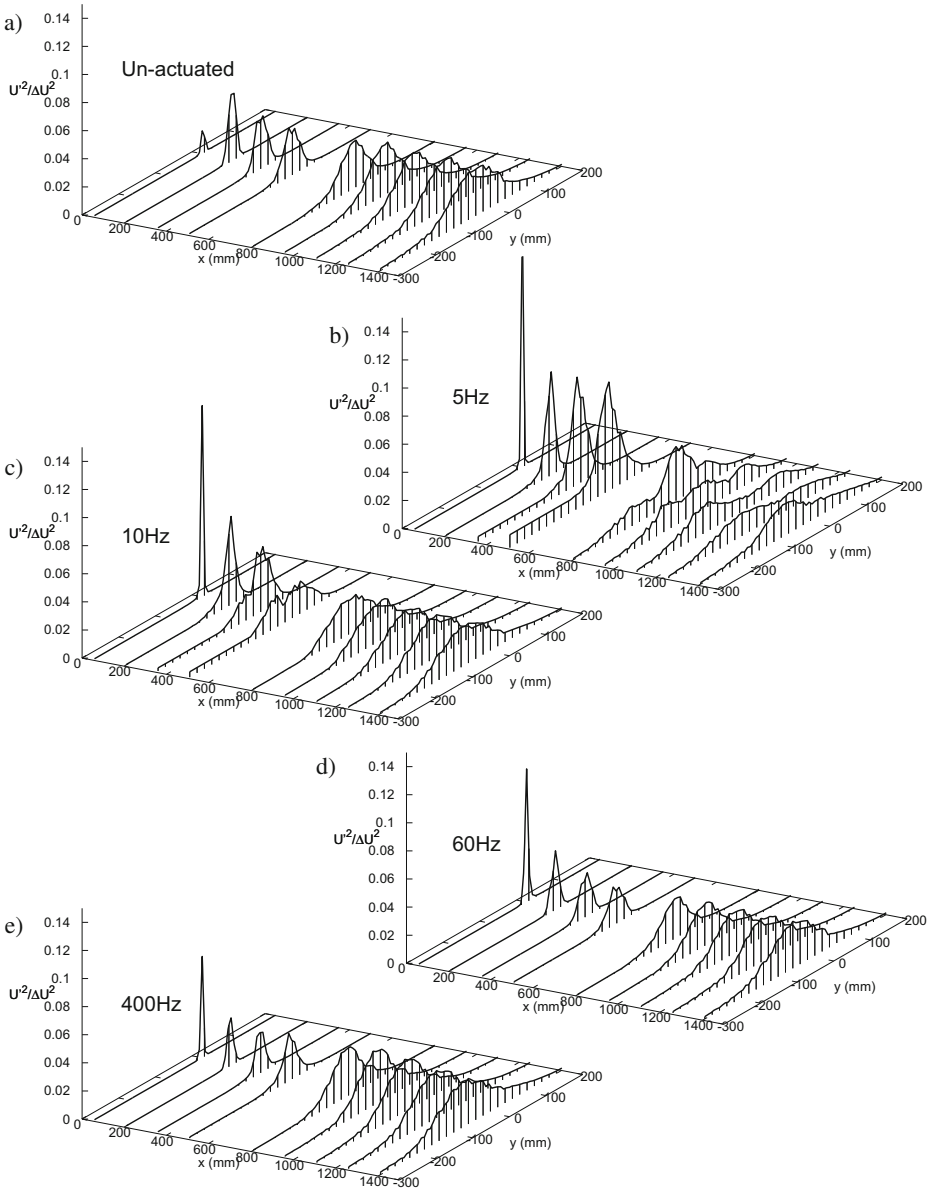

Fig. 7 Evolution of $\overline{u'^2}/\Delta U^2$ for: **a**) un-actuated flow, **b**) $f_a = 5$ Hz, **c**) $f_a = 10$ Hz, **d**) $f_a = 60$ Hz, **e**) $f_a = 400$ Hz

for this case, a resurgence of a single-peak profile can be observed, which indicates that far enough downstream this configuration will establish a growth rate similar to the un-actuated flow, just as is the case with $f_a = 10$Hz in Fig. 7c between $x = 500$mm and $x = 800$mm.

Compared to the un-actuated flow, actuation with $f_a = 60$Hz and $f_a = 400$Hz reduces the initial fluctuation energy as can be seen in Fig. 7(d) and (e), respectively. This corresponds to the reduced initial vorticity thickness growth rate, as seen in Fig. 5. High actuation frequency is not able to synchronize the mixing layer as low actuation frequencies do; instead the momentum injected in this way into the mixing layer diffuses as a part of the turbulence cascade. It should be noted that actuation at $f_a = f_{KH}$ produced results very similar to $f_a = 400$Hz.

The response of the mixing layer to open-loop forcing was then explored in detail for two stream-wise measurement positions, to create a base of reference for local frequency selection. In order to truncate the experimental time needed for complete mapping of the frequency/duty cycle space, the actuation was limited to a 50 % duty cycle and frequencies of $1\text{Hz} < f_a < 500\text{Hz}$, applied in steps of $\Delta f_a = 1$Hz. The results can be observed in Fig. 8 as the objective function normalized by the un-actuated flow value J_u for each actuation frequency. We can see that actuating in low band ($f_a \ll f_{KH}$) provokes an increase of J/J_u. At $x = 200$mm, a maximum of $(J/J_u)\,\text{max} = 2.5$ is obtained for $f_a = 14$Hz. Using high band actuation ($f_a > f_{KH}$) results in $J/J_u < 1$. When measuring further downstream, at $x = 500$mm, a maximum of $(J/J_u)\,\text{max} = 3.2$ corresponds to $f_a = 4$Hz. In this case, a minimum of J/J_u can be observed around $f_a = 60$Hz.

It is important to note that the best actuation frequencies for maximization of J/J_u are unique for different measurement locations. If the best actuation frequency $f_a = 14$Hz for $x = 200$mm is applied when measurements are taken at $x = 500$mm, the objective function is not optimally enhanced, as shown in Fig. 8.

4 Closed-Loop Control

In this section, we present experiments with three different closed-loop approaches. A classical extremum-seeking adaptive control (Section 4.1) is applied to detect the optimal

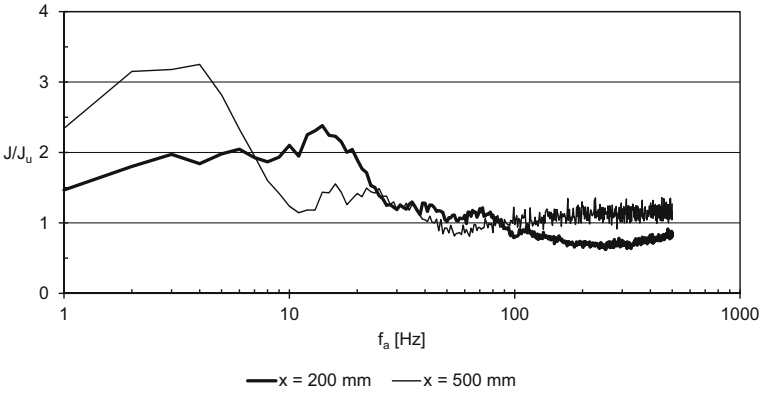

Fig. 8 Normalized objective function J/J_u for $1\text{ Hz} < f_a < 500$ Hz, where actuation frequency is varied in steps of $\Delta f_a = 1$ Hz (shown in logarithmic scale). Thick line denotes results for sensors at $x = 200$ mm and thin line for $x = 500$ mm

frequency of actuation at $x = 200$mm. A simple POD mode feedback control (Section 4.2) is used to distill and directly feed back an actuation signal based on the intrinsic information contained in the mixing layer at $x = 200$mm or $x = 500$mm. Finally, machine learning control (Section 4.3) is employed to find an optimal solution for maximizing the objective function J at $x = 200$mm using velocity fluctuation signals as variables for the generated control law.

4.1 Extremum seeking control

Extremum-seeking is an adaptive control strategy that is ideal for finding the minimum or maximum value of an objective function for a dynamical system that is nonlinear and may be difficult to characterize [12, 13]. Many tools in feedback control theory only apply to linear systems or linearized systems near a fixed point. In contrast, Extremum-Seeking Control (ESC) is a model-free method, and recent results establish conditions for stable convergence, even with nonlinear systems [13]. ESC has been applied to a wide range of problems in fluid mechanics and electrical engineering. The underlying principle of ESC is the injection of a sinusoidal perturbation signal, which passes through the nonlinear system and results in a sinusoidal output perturbation of the objective, perhaps with a phase delay. The demodulated signal obtained by multiplying the input and output perturbations provides an estimate of the gradient of the objective function in the input variable, which is larger away from the extremum point of a quadratic objective function. This signal may then be added to the best guess for the maximizing (or minimizing) input, causing the estimate to move towards the local maximum (or minimum). There are a number of engineering practicalities that arise when designing an extremum-seeking controller. First, the time-scale of the dynamics must be fast with respect to the sinusoidal perturbation, so that transients relax and we obtain a sinusoidal output perturbation. In addition, the amplitude of the input perturbation must be large enough to provide a decent signal-to-noise ratio. Finally, the method only finds the local maximum of a objective function, and it may be necessary to design a larger input amplitude to average over local maxima in the objective function. Because of the time-delays and nonlinearities in the underlying system, it may be necessary to include a time-delay on the input signal when demodulating with the high-pass filtered output perturbation.

In the experiment, the input variable is the actuation frequency f_a; we vary this actuation frequency sinusoidally, with an amplitude A and frequency f_mod, so that $f_\mathrm{a}(t) = \hat{f}_\mathrm{a} + An(f_\mathrm{mod}t)$. As mentioned in Section 2, measurements are made over a window of 10 seconds for the objective function evaluation. This establishes an effective time delay of 10 seconds, which we incorporate into the input perturbation for the demodulation step. This also determines the *fast* timescale on which the objective function transiences change with changing inputs. We therefore choose an oscillation frequency on f_a of $f_\mathrm{mod} = 1/20$Hz, which is slower compared with the averaging window.

Results of searching for a maximum of J with a modulation amplitude of $A = 2$Hz are shown in Fig. 9. The initial actuation frequency is a sub-optimal value, and the ESC manages to converge to an optimal solution of $f_\mathrm{a} = 14$Hz after a little less than 300 seconds. However, the initial frequency $f_\mathrm{a} = 26$Hz is close to the maximum and from Fig. 8 (for $x = 200$mm) a well defined slope is observed between these two points which significantly simplifies the task for the ESC. Attempts to find the global maximum from an initial point in frequency space more distant from the target, have necessitated the use of greater

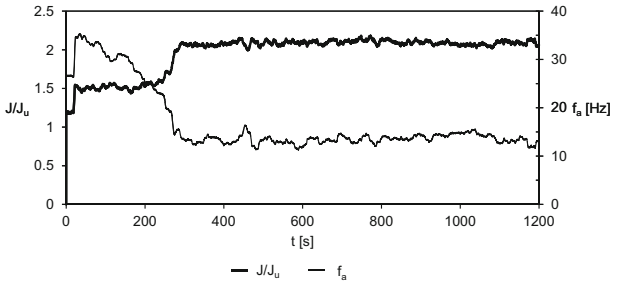

Fig. 9 Maximum seeking control at $x = 200$ mm: convergence of J and actuation frequency f_a

modulation amplitudes up to $A = 10$Hz. The larger oscillation amplitudes provide more robust convergence to the global maximum (because small local maxima are averaged out), but with more steady-state perturbation errors.

4.2 POD mode feedback control

The Proper Orthogonal Decomposition (POD) of the sensor signals in real time can provide efficient feedback information for a closed-loop control as shown in [7]. POD analysis reveals an energy-based composition of a flow. The aim is to generate a feedback control signal, based on the time series of the most energetic POD mode, which would automatically contain the optimum frequency that will synchronize and enhance this mode in the mixing layer. Amplification of the energetically most dominant mode should lead to maximization of the energy-based objective function at a given location.

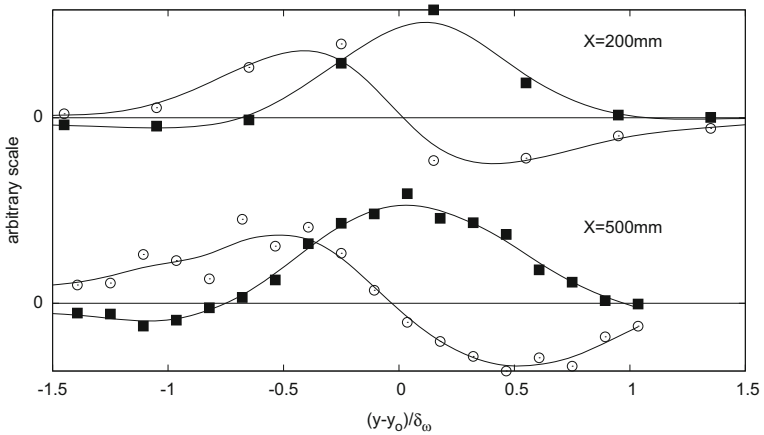

Fig. 10 First two POD modes of the fluctuating velocity obtained in the un-actuated case, using the hot-wire rake. POD mode 1 (closed symbols) and POD mode 2 (open symbols) are plotted on a scale normalized by the local vorticity thickness for $x = 200$ mm (top) and $x = 500$ mm (bottom), with y_0 corresponding to the local coordinate of the mean velocity profile inflexion point

For a selected stream-wise location x of the hot-wire rake, a POD is first performed on a time history of velocity fluctuations $u'(y_i, t)$ of the un-actuated flow. These signals are decomposed as:

$$u'^{\mathrm{u}}(y_i, t) = \sum_{n=1}^{N} a_n^{\mathrm{u}}(t)\, \Phi_n^{\mathrm{u}}(y_i), \tag{3}$$

where N, the number of POD modes, corresponds to the number of hot-wires used in the rake. Real time velocity signals can then be projected onto a given POD mode Φ_n^{u} in such a way that a real-time estimate of the contribution of this mode (a projection coefficient) $a_n(t)$ is obtained as:

$$a_n(t) = \sum_{i=1}^{N} u'(y_i, t)\, \Phi_n^{\mathrm{u}}(y_i). \tag{4}$$

Figure 10 illustrates the shapes of the first two POD modes, *i.e.* the two most energetic ones, that were obtained at the stream-wise locations $x = 200$mm and $x = 500$mm. For both stream-wise positions, the shapes of these modes are similar. Mode 1 is an even function of y and exhibits one maximum located close to the local mixing layer axis while mode 2 crosses zero at this location and is an odd function of y. In terms of instantaneous flow organization, these modes are then related to two different topologies of the fluctuation velocity field. Mode 1 is more representative of the mixing layer inner region, close to the mixing layer axis, while mode 2 is more representative of convected large scales structures

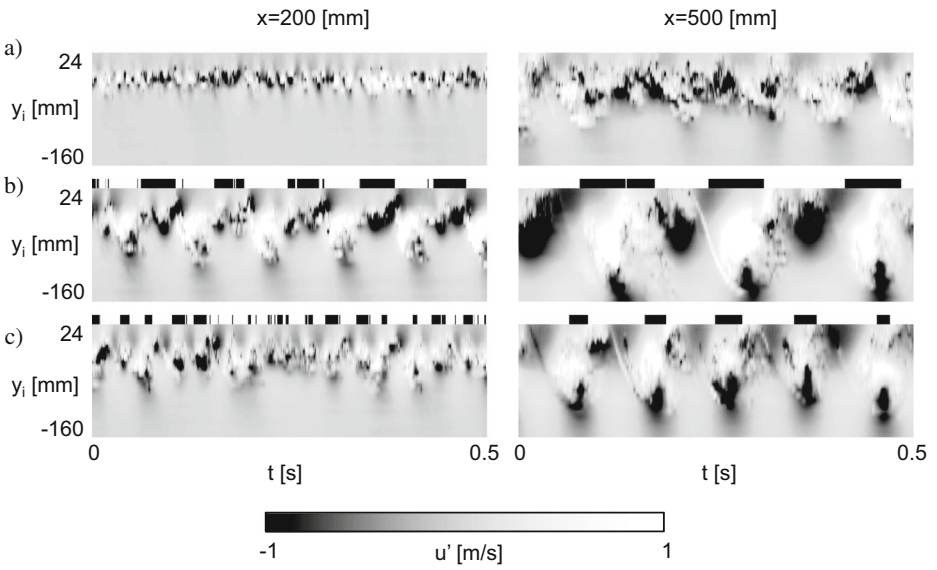

Fig. 11 Pseudo flow visualizations at $x = 200$ mm and $x = 500$ mm. Greyscale maps correspond to iso levels of the time history of the fluctuating velocity from the hot-wire rake. The vertical direction corresponds to the hot-wire probe y_i position. The horizontal direction corresponds to time (0.5 s), plotted from right to left, following a Taylor's hypothesis, to match a spatial organization. Fields indicate **a**) un-actuated flow, **b**) POD feedback control using mode 1, **c**) POD feedback control using mode 2. Black rectangular fields above each greyscale map indicate actuation (black for active)

and the spatial anti-phase relationship they create between the two outer limits of the mixing layer [3].

A threshold denoted a_{thr} is introduced such that for $a_1(t) > a_{\text{thr}}$ the actuators are open. This threshold is tuned manually in such a way that a synchronization appears. This strategy has been applied successfully to the mixing layer as illustrated in Fig. 11. From the visualizations of the un-actuated configuration (Fig. 11a) no specific low-frequency/large-scale organization of the flow is apparent. When the feedback is applied, based on mode 1, the resulting flow (shown in Fig. 11b) is very well synchronized by a *self-triggering mode* at a characteristic frequency naturally present at this particular stream-wise location. A spectral analysis of the feedback signal leads to a dominant frequency $f_a \approx 10$Hz and $f_a \approx 6$Hz at locations $x = 200$mm and $x = 500$mm, respectively. When mode 2 is used to drive the actuators (Fig. 11c), dominant frequencies are found to be $f_a \approx 15$Hz and $f_a \approx 10$Hz, for the corresponding stream-wise locations. These results show that mode 1 and 2 do not synchronize at the same frequency: mode 1 leads to a frequency that is of the order of 2/3 of that of mode 2. It is remarkable that such a ratio, previously observed for a natural turbulent mixing layer [3], exists in the case of a forced mixing layer. The best obtained values of the objective function, using mode 1 actuation, are $(J/J_u)_{POD} = 2.65$ at $x = 200$mm, and $(J/J_u)_{POD} = 2.74$ at $x = 500$mm.

These experiments show that a feedback control can take into account the local flow information at a given downstream location. Furthermore, such control gives rise to a significant increase of the local turbulent activity and leads to a possible self-triggering synchronization of the flow. The key feature in obtaining the optimal actuation using POD

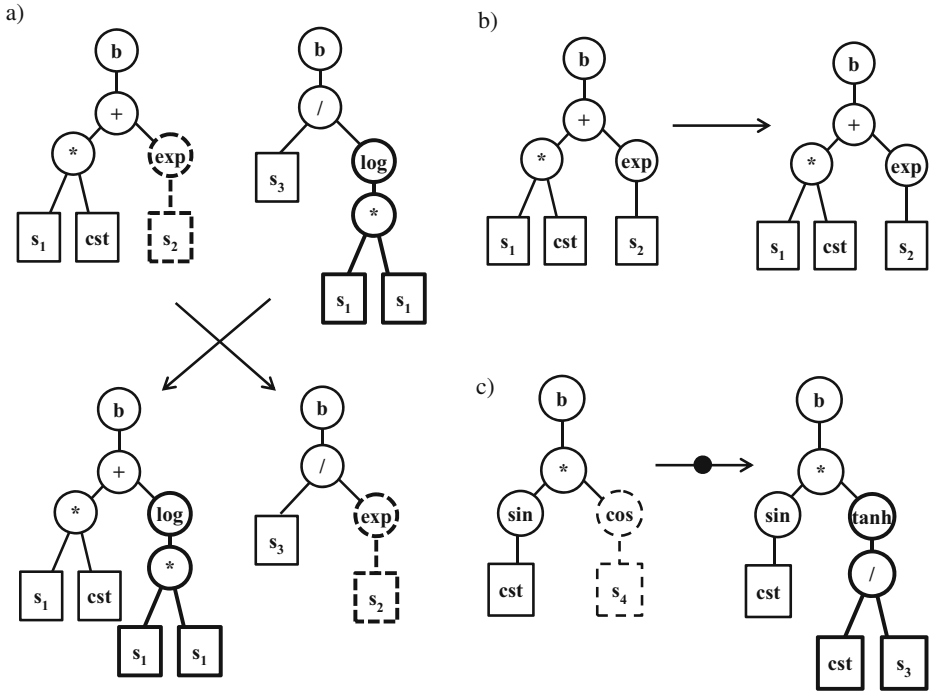

Fig. 12 Bio-inspired operations performed by Genetic Programming (GP) on the tree-like functions, in the process of looking for the best individual. **a**) Cross-over, **b**) replication and **c**) mutation

modes is the selection of the threshold for the generation of the actuation signal. A process is needed where such optimization would be automatically obtained.

4.3 Machine learning control

For determining an optimal control law, we propose a model-free control design using the tools from machine learning [18], in particular the Genetic Programming (GP) [10, 11] technique. GP is a biologically inspired [23] function optimization method. The best control law is searched iteratively as a composition of elementary functions of constants and sensor signals. A objective function, pertinent to the problem in question, grades how a given control law performs. This objective function can be formulated to put the system in a desirable state or to maximize (or minimize) a given measure of the system, such as the turbulent kinetic energy (our case). A first set of control law candidates (called individuals) is generated through random composition of the elementary functions and constants. The exploited GP algorithm [15] combines these operations in the form of a tree (see examples in Fig. 12), which allows it to generate any linear or non-linear function in order to build the initial generation of individuals. Each individual is attributed a objective through the evaluation of J defined in Eq. 1. The next set of individuals (called generation) is generated through mutation, cross-over or replication of individuals with a specific rate for each process. These operations are illustrated in Fig. 12. Typically for genetic programming, a global extremum of the objective function is obtained in 50 generations, provided that the population of each contains enough diversity for the algorithm to exploit. There is no general mathematical proof for convergence but the method has been proved successful [14, 19].

The current MLC code uses constant-size populations. Population size can range from 100 up to 1000 individuals for each generation, depending on the experiment. The goal is to find an individual for a maximization of the objective function J. Functions used comprise $(+, -, \times, /, n, \cos, \exp, \log, \tanh)$, with up to 24 hot-wire probe velocity fluctuation signals $u_i'(t)$ as variables and values from a range of [-1:1] are available to be selected as constants. The value returned by the control function is compared to a threshold of 0 so that the micro-valves are turned on when the value is above the threshold and off otherwise. The GP process is set to run until the 50th generation, after which the best individual is selected.

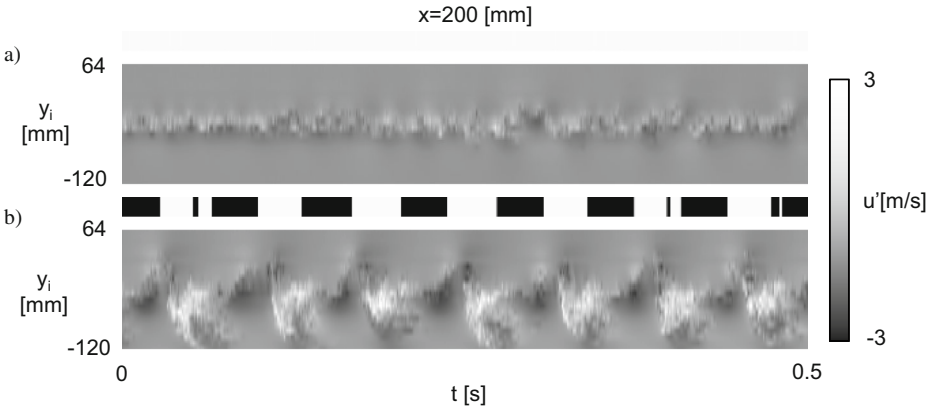

Fig. 13 Pseudo-visualization of the reference un-actuated flow (**a**), and the best MLC individual (**b**), for maximization of J at $x = 200$ mm. Black fields on top of the visualization represent actuation

Choosing the best individual from the last generation of the GP testing run effectively means that the MLC learning phase is finished and the obtained function can be applied for a continuous closed-loop control of the flow.

Figure 13 shows the reference un-actuated flow and the resulting best individual of an MLC experiment with sensors placed at $x = 200$mm. MLC has found the same mechanism of self-synchronization of the flow at a local characteristic frequency (as in Section 4.2), with a normalized objective function value of $(J/J_u)_{MLC} = 2.59$. The spectral analysis yields a frequency of around 14Hz. The actuation properties of the best MLC individual correspond very well to the best open-loop frequency (Fig. 8) and the best ESC solution (Fig. 9). This control law was obtained without using any a priori knowledge of the system response. The open-loop reference is only used to confirm that the process converged on an optimal solution. Compared to the POD feedback control, the actuation signal of the best MLC control law incorporates automatically an optimal relationship with regard to the threshold for actuation signal generation. If it were not so, this control law would not have the best performance and would not have been selected. We can conclude that MLC has provided the optimization process missing in the POD feedback control. A coupling of these two methods may provide further improvements.

5 Conclusions

The experimental investigation shows good control authority of the actuator system on the basic features of the mixing layer. The actuation provokes different effects on the mixing layer properties with regard to its stream-wise evolution. The initial "perturbed" part of the mixing layer will experience either an increased (up to double) or a decreased vorticity thickness growth rate. For a given frequency of actuation, the flow will be synchronized at f_a up to a stream-wise location at which the local natural frequency of the un-actuated flow is approximately f_a. At this point the mixing layer begins a transition into a state similar to the un-actuated flow corresponding to this point, and adopts a growth rate of the un-actuated flow (but not necessarily the same local vorticity thickness).

An extremum seeking control is applied based on the mapping of the mixing layer responsiveness to periodic forcing on a wide range of frequencies allowed by design limits of the actuation system. While this type of control has no problem of reaching local maxima, the complexity of the response amplitudes makes it difficult to know whether a global maximum has been reached. Finding a global maximum requires initially a very high amplitude of actuating frequency modulation which reduces the steadiness of the solution once it has been reached.

It should be noted that sensor-based closed-loop control is *per se* not necessarily performing better than periodic forcing. There is no guarantee that this closed-loop control can emulate, for instance, a periodic clock-work of actuation. Closed-loop control performance may be mitigated by time-delays, noise amplifications, etc. We explore the possibilities of closed-loop control using two approaches; one based on physical insight and another based on machine learning which by definition requires no *a priori* knowledge.

A simple feedback approach was tested, where the local organization of the flow obtained by a POD approach at a given stream-wise location is used to trigger the perturbations. A synchronization occurs that enhances this local organization, and comes as a direct consequence of the natural spatial selection of the dominant frequency of the flow, inherent in the unperturbed mixing layer. This effectively means that with this type of feedback control no previous frequency sweep is necessary for revealing the optimal parameters; the flow

itself will feed back the optimal actuation frequency. This self-synchronization constitutes a simple mechanism in otherwise highly non-linear problem, and is known as a fundamental phenomenon in dynamical systems [22].

Finally, a model-free machine learning control method, as exemplified for a non-linear dynamic system [4] is proven capable of finding and exploiting the same intrinsic information in the flow that were observed in the POD mode feedback experiment, but using directly velocity signals from several sensors. The difference is that while the threshold of actuation imposed on POD mode feedback signal needs to be carefully adjusted by hand, the MLC will create the best individual which already contains this kind of optimization. An even more interesting possibility is to use POD modes as variables in MLC instead or even in parallel with velocity fluctuations. In this case, the MLC process will determine which kind of signal is best used for obtaining a given objective.

The success of feedback control approaches implies that we can harness the information directly from the flow in order to create a desired control input. This is even of more importance when we consider that the control of a turbulent mixing layer involves highly non-linear dynamics, which are difficult to model with currently available methods. It also removes the need for parametric studies of open-loop actuation for different flow regimes. A systematic search of the best actuation amplitude, frequency and duty cycle is a lengthy process even for one set of initial flow conditions, let alone for an entire range of velocities to which the control would have to respond if applied to a practical engineering problem. As shown in this article, an optimal open-loop actuation for one stream-wise sensor position ($x = 200$mm) is significantly under-performing when used for maximization of the objective function for a different sensor position ($x = 500$mm). Contrary to this, the POD feedback control, using the same mode, is capable of auto-adapting and producing effective maximization of the objective function for both stream-wise locations tested.

The POD analysis provides the information needed for local synchronization of the mixing layer at different stream-wise measurement locations. The MLC can use such information in order to find the most efficient control law. Development of the MLC method continues by introducing new types of variables and by optimization of the time needed to converge on the best control law solution. In perspective, one can envisage a multitude of different filtering approaches applied on the sensor signals and using the resulting functions as variables in MLC. Additionally, time can be introduced as an input variable. This would enable an automatic MLC based optimization of open-loop control when closed-loop control is less effective.

Ongoing experimental campaigns will deal with stabilization of the mixing layer using MLC, testing of robustness of best individuals to different initial conditions or perturbations and exploring different stream-wise locations. The authors are also actively pursuing the application of this method in several other experiments. For more in-depth information on MLC we kindly invite the reader to look at [4].

Acknowledgments The authors acknowledge the funding and excellent working conditions of the Senior Chair of Excellence 'Closed-loop control of turbulent shear flows using reduced-order models' (TUCOROM) supported by the French Agence Nationale de la Recherche (ANR) and hosted by Institute PPRIME. The work is also supported by the ANR grant SepaCoDe. Marc Segond would like to acknowledge the support of the LINC project (no. 289447) funded by ECs Marie-Curie ITN program (FP7-PEOPLE-2011-ITN). We thank the Ambrosys Ltd. Society for Complex Systems Management, the Bernd Noack Cybernetics Foundation and Hermine Freienstein-Witt for additional support. We appreciate valuable stimulating discussions with the TUCOROM team: Jean-Luc Aider, Jacques Borée, Nicolas Gautier, Eurika Kaiser, Michael Schlegel, and the SepaCoDe team headed by Azzedine Kourta and Michel Stanislas. Special thanks are due to Nadia Maamar for a wonderful job in hosting the TUCOROM visitors.

References

1. Cattafesta, L.N.I., Sheplak, M.: Actuators for active flow control. Annu. Rev. Fluid Mech. **43**, 247–272 (2011)
2. Corke, T.C., Enloe, C.L., Wilkinson, S.P.: Dielectric barrier discharge plasma actuators for flow control. Annu. Rev. Fluid Mech. **42**, 505–529 (2010)
3. Delville, J., Ukeiley, L., Cordier, L., Bonnet, J.P., Glauser, M.: Examination of large-scale structures in a turbulent plane mixing layer. Part 1. Proper orthogonal decomposition. J. Fluid Mech. **391**, 91–122 (1999)
4. Duriez, T., Parezanović, V., Cordier, L., Noack, B.R., Delville, J., Bonnet, J.P., Segond, M., Abel, M.: Closed-loop turbulence control using machine learning. Submitted to J. Fluid Mech. Available in preprint on arXiv (2014)
5. Fiedler, H.E.: Control of free turbulent shear flows. In: Flow Control: Fundamentals and Practices, Lecture Notes in Physics Monographs, vol. 53, pp. 335–429. Springer-Verlag (1998). ISBN 3-540-63936-5
6. Gautier, N., Aider, J.L., Duriez, T., Noack, B.R., Segond, M., Abel, M.: Closed-loop separation control using machine learning. Submitted to J. Fluid Mech. Available on arXiv (2014)
7. Glauser, M., Higuchi, H., Ausseur, J., Pinier, J., Carlson, H.: Feedback control of separated flows. In: 2nd AIAA Flow Control Conference (2004)
8. Glezer, A., Amitay, M.: Synthetic jets. Annu. Rev. Fluid Mech **34**, 503–529 (2002)
9. Ho, C.M., Huerre, P.: Perturbed Free Shear Layers. Annu. Rev. Fluid Mech. **16**, 365–424 (1984)
10. Koza, J.R.: Genetic Programming: on the Programming of Computers by means of Natural Selection, vol. 1. MIT Press (1992)
11. Koza, J.R., Bennett, F.H. III., Stielman, O.: Genetic programming as a Darwinian invention machine. In: Genetic Programming, pp. 93–108. Springer (1999)
12. Ariyur, K.B., Krstić, M.: Real-time Optimization by Extremum-seeking Control. John Wiley & Sons (2003)
13. Krstić, M., Wang, H.H.: Stability of extremum seeking feedback for general nonlinear dynamic systems. Automatica **36**, 595–601 (2000)
14. Lewis, M.A., Fagg, A.H., Solidum, A., Bekey, G.A.: Genetic programming approach to the construction of a neural network for control of a walking robot. In: IEEE Conference on Robotics and Automation, pp. 2618–2623 (1992)
15. Luke, S., Panait, L., Balan, G., Paus, S., Skolicki, Z., Kicinger, R., Popovici, E., Sullivan, K., Harrison, J., Bassett, J., et al.: A Java-based Evolutionary Computation Research System (1993). http://cs.gmu.edu/eclab/projects/ecj/
16. Lumley, J.L.: Atmospheric Turbulence and Wave Propagation. The Structure of Inhomogeneous Turbulence, pp. 166–178. Nauka, Moscow (1967)
17. Mathis, R.: Etude Expérimentale du Contrôle d'une Couche de Mélange par Décollement Piloté. Phd thesis, Université de Poitiers (2006)
18. Murphy, K.P.: Machine Learning: A Probabilistic Perspective. MIT Press, Cambridge (2012)
19. Nordin, P., Banzhaf, W.: An on-line method to evolve behavior and to control a miniature robot in real time with genetic programming. Adapt. Behav. **5**(2), 107–140 (1997)
20. Oster, D., Wygnanski, I.: The forced mixing layer between parallel streams. J. Fluid Mech. **123**, 91–130 (1982)
21. Perret, L.: Etude du couplage instationnaire calculs-expériences en écoulements turbulents. Phd thesis, Université de Poitiers (2004)
22. Pikovsky, A., Rosenblum, M., Kurths, J.: Synchronization: a Universal Concept in Nonlinear sciences. Cambridge University Press, Cambridge (2001)
23. Wahde, M.: Biologically Inspired Optimization Methods: an Introduction. WIT Press (2008)
24. Wiltse, J.M., Glezer, A.: Manipulation of free shear flows using piezoelectric actuators. J. Fluid Mech. **249**, 261–285 (1993)